International Journal of Heat and Mass Transfer 122 (2018) 45–58

Contents lists available at ScienceDirect

International Journal of Heat and Mass Transfer

journal homepage: www.elsevier.com/locate/ijhmt

Mode selection between sliding and rolling for droplet on inclined surface: Effect of surface wettability

Jian Xie [a], Jinliang Xu [a,*], Wei Shang [a], Kai Zhang [b]

[a] Beijing Key Laboratory of Multiphase Flow and Heat Transfer for Low Energy Utilization, North China Electric Power University, Beijing 102206, PR China
[b] Beijing Key Laboratory of Emission Surveillance and Control for Thermal Power Generation, North China Electric Power University, Beijing 102206, PR China

ARTICLE INFO

Article history:
Received 16 October 2017
Received in revised form 20 January 2018
Accepted 21 January 2018

Keywords:
Wettability
Contact angle
Sliding or rolling
Dropwise condensation
Fuel cell

ABSTRACT

Onset of droplet motion is important for various applications, including dropwise condensation and water management in fuel cells. In order to determine critical conditions for onset of motion and specific motion mode, a general problem having a droplet sheared by a gas stream on inclined surface is investigated. Two criterion equations are theoretically established for onset of droplet sliding and rolling independently, including dimensionless parameters of Bond number (*Bn*), Ohnesorge number (*Oh*) and Weber number (*We*), inclination angle parameter and wettability parameters. The criterion equations predict critical gas velocity, maximum droplet radius, and "sliding angle" or "rolling angle". Droplet sliding predictions agree well with experimental data in the literature. Criterion surfaces of sliding or rolling are constructed to verify if sliding or rolling can be initiated, influenced by both equilibrium contact angle and contact angle hysteresis. By coupling the criterion equations of sliding and rolling, we develop a mode selection criterion equation, which is only dependent on equilibrium contact angle θ_e. Three regions are clarified: (1) for $126.3° < \theta_e < 147.0°$, a droplet rolls if $Bn < Bn_t$ and slides if $Bn > Bn_t$, where Bn_t is the transition Bond number; (2) for $\theta_e < 126.3°$, a droplet only slides; (3) for $\theta_e > 147.0°$, a droplet only rolls. The theoretically determined 147.0° contact angle is newly recommended as the contact angle boundary between hydrophobicity and super-hydrophobicity. One of the applications of this work is to provide a general guideline for droplet detachment or retention in fuel cells and condensers.

1. Introduction

The determination of critical condition for droplet detachment on inclined surface is important for many natural phenomena and engineering applications. In arid and semiarid environments, leaf hydrophobicity of plant species is important for rain droplet detachment to increase water availability for soil [1]. On the other hand, tank-mix adjuvants are used to improve the efficiency of foliage applied pesticide formulations, especially if they are used at reduced dose rates. In this context, liquid retention on leaf surfaces is the desired outcome [2–4].

Water management is important in polymer electrolyte fuel cells (PEFCs) and proton exchange membrane fuel cells (PEMFCs): appropriate humidification is critical to achieve high ionic conductivity of membrane but excessive water causes flooding and consequently reduces cell performance [5,6]. Water droplets occur on hydrophobic gas diffusion layer (GDL) surfaces and hinder the transport of oxygen and hydrogen towards respective catalyst layers where the electrochemical reactions occur. Droplets should be removed in a suitable gas shearing flow.

Dropwise condensation on hydrophobic surface improves condenser performance. Droplet nucleation, growth and detachment are key to affect condensation heat transfer. Two droplet sizes should be included in condensation heat transfer model [7,8]: minimum drop radius at which a drop initiates nucleating (r_{min}), which is beyond the scope of this paper, and maximum droplet radius at which a droplet initiate moving, r_{max}, which is the scope of this paper.

Considering a droplet sheared by a gas stream on inclined surface, there are four possible detachment modes: sliding mode in which the relative position between any two liquid particles is not changed (see Fig. 1a), rolling mode for a droplet rotating (see Fig. 1b), lifting mode to float a droplet (see Fig. 1c), and dripping mode to make a droplet falling down (see Fig. 1d). Physically, the critical condition at which a droplet begins to move depends on the deformed droplet induced surface tension force competed by gravity force and/or shear force for sliding, lifting and dripping modes. Alternatively, the critical rolling condition depends on the competition of various forces induced torques.

* Corresponding author.
E-mail address: xjl@ncepu.edu.cn (J. Xu).

https://doi.org/10.1016/j.ijheatmasstransfer.2018.01.098
0017-9310/

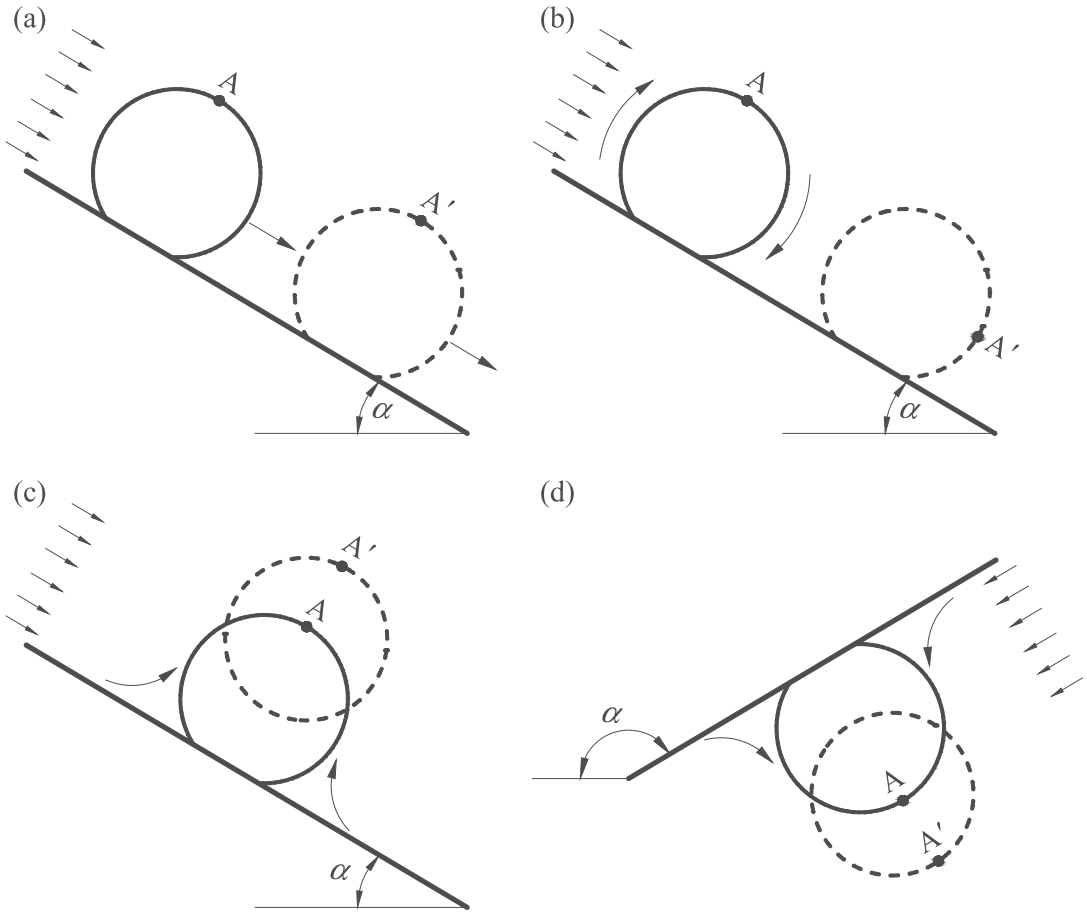

Fig. 1. The four droplet detachment modes on inclined surface (a: sliding, b: rolling, c: lifting, and d: dripping).

Table 1 summarized droplet detachment studies in the literature. Even though some sliding investigations are reported, droplet sliding under comprehensive effects of surface tension force, shear force and gravity force is not well understood. For example, Chen [9], Cho et al. [10] and Fan et al. [11] treated sliding motion under the effects of shear force and surface tension force, without considering gravity force due to the horizontal surface used. Alternatively, Dimitrakopoulos and Higdon [12] treated sliding motion with surface tension force competed only by gravity force without shear force effect.

Steady droplet rolling after its initiation has been investigated previously. Richard and Quere [13] determined the relationship between rolling velocities and droplet sizes. They found that the rolling velocity is constant for droplet radius larger than the capillary length, but is increased with the decrease of droplet radius for droplet radius smaller than the capillary length. Richard and Quere

Table 1
Literature review on droplet detachment.

Refs.	Applications	Detachment modes	Shear effect	Gravity effect	Results and comments
Chen [9]	PEMFC or PEFC	Sliding	Yes	No	Force balance analysis is used to predict critical gas velocity for drop sliding with fixed drop size in the horizontal gas diffusion layer (GDL).
Cho et al. [10]	PEFC	Sliding	Yes	No	Non-dimensional equation was obtained by forces balance in the horizontal GDL.
Fan et al. [11]	–	Sliding	Yes	No	Critical gas velocity shearing a droplet in a horizontal channel was measured, with four drop sizes, three types of surfaces and three liquids. Static, advancing and receding contact angles were given for each run, which are useful for comparison with theoretical/numerical studies.
Dimitrakopoulos and Higdon [12]	–	Sliding	No	Yes	Non-dimensional equation is obtained by forces balance parallel to the titled wall surface.
Qi et al. [18]	Dropwise condensation	Rolling	No	Yes	Critical detachment drop size for rolling was obtained by balancing moment equilibrium on vertical surface.
Ran et al. [19]	Wettability characterization	Rolling	No	Yes	Moment equilibrium analysis is used to predict critical rolling angel of titled surface for drop detachment.
Sikarwar et al. [7]	Dropwise condensation	Sliding and dripping	No	Yes	Critical sliding drop size is obtained by balancing forces parallel to titled surface. Critical dripping drop size is obtained by balancing forces perpendicular to titled surface.
Basu et al. [20]	–	Sliding and lifting	Yes	No	Critical sliding drop size is obtained by balancing forces parallel to horizontal surface. Critical lifting drop size is obtained by balancing forces perpendicular to surface. The authors show that sliding is preferred than lifting.

[13]'s experimental finding was further explained by Mahadevan and Pomeau [14]'s theoretical analysis. Similar conclusion was drawn by Yilbas et al. [15] using numerical simulation. Thampi et al. [16] identified a universal curve for the amount of rotation velocity inside the drop as a function of the drop shape characterized by the isoperimetric quotient. Wind-Willassen and Sorensen [17] found that the behavior of the drop velocity can be a function of the slip length.

Fewer investigations can be found to determine critical conditions for onset of rolling, lifting and dripping. To deal with rolling mode, Qi et al. [18] and Ran et al. [19] considered adhesion work competed by gravity force induced torque. Basu et al. [20] is one of few references to tackle droplet lifting, in which they stated that lifting is more difficult to occur than sliding.

The objective of this paper is to develop critical criterions for onset of sliding and rolling. A droplet sheared by a gas stream is dealt with as a general problem, including comprehensive effects of surface tension force, gravity force and shear force. The independently developed criterion equations are expressed in non-dimensional form to reflect relative contribution of various factors on sliding and rolling. By coupling critical criterion equations of sliding and rolling, a mode selection criterion equation is constructed to determine specific mode once a droplet can move. It is shown that the mode selection is only dependent on equilibrium contact angles. Three regions are identified to have $\theta_e > 147.0°$ for rolling only, $\theta_e < 126.3°$ for sliding only, and $126.3° < \theta_e < 147.0°$ for pending mode, depending on Bond number.

The major contribution of this work is the determination of the motion mode, sliding or rolling, once the droplet can move. The motion mode selection is of significant interest to the wetting community. The droplet dynamics poses an interesting question, viz. whether a liquid drop sitting on an inclined solid surface will roll, slide, or do both [16], which has not been solved yet. This problem is thoroughly investigated in this paper.

2. Problem statement and parameters definitions

Fig. 2 shows the studied problem. A gas stream flows in a rectangular channel. The gas flow direction is parallel to the channel wall, having the tendency to move a droplet on the wall. For the channel height (H) sufficiently smaller than the channel width, a two-dimensional gas flow is assumed. The channel has an inclination angle α with respect to horizontal direction, in which $\alpha = 0°$, $\alpha = 90°$ and $\alpha = 180°$ refer to a droplet above a horizontal wall, on a vertical wall, below a horizontal wall, respectively. The droplet height is h, which is much smaller than H, usually. Thus, effect of pressure difference between droplet upstream and downstream can be neglected [21]. The droplet may be deformed, with an advancing contact angle θ_a and a receding contact angle θ_r. For fully developed laminar channel flow, the average gas velocity in a droplet height h is [22]

$$\overline{U}_h = \frac{\overline{U}_H h}{H^2}(3H - 2h). \tag{1}$$

For fully developed turbulent channel flow, gas velocities have linear distribution in the viscosity sub-layer, but have exponent distribution in the bulk flow region [23]:

$$\frac{U(y)}{U^*} = \begin{cases} \frac{yU^*}{\nu}, & 0 \leqslant y < \delta, \\ \frac{1}{k}\ln\frac{yU^*}{\nu} + C, & \delta \leqslant y < \frac{H}{2}, \\ \frac{1}{k}\ln\frac{(H-y)U^*}{\nu} + C, & \frac{H}{2} \leqslant y < H-\delta, \\ \frac{(H-y)U^*}{\nu}, & H-\delta \leqslant y \leqslant H. \end{cases} \tag{2}$$

In Eq. (2), U^* is shear stress velocity, ν is kinematic viscosity, δ is viscosity sub-layer thickness, k and C are constants: $k = 0.4$, $C = 5.5$. Because velocities should be continued at $y = \delta$, Eq. (2) yields the following equation at $y = \delta$:

$$\delta = \frac{11.6\nu}{U^*}. \tag{3}$$

The average gas velocity in the whole channel height H is

$$\begin{aligned} \overline{U}_H &= \frac{1}{H}\int_0^H U(y)dy \\ &= \frac{\delta^2 U^{*2}}{H\nu} + \frac{U^*}{k}\ln\frac{H}{4\delta} + \frac{(H-2\delta)U^*}{Hk}\left(\ln\frac{\delta U^*}{\nu} + kC - 1\right). \end{aligned} \tag{4}$$

Eq. (4) quantifies the relationship between $\overline{U}_H$ and U^*. Integrating Eq. (4) over the droplet height h, one yields the relationship between $\overline{U}_h$ and U^* as

$$\overline{U}_h = \begin{cases} \frac{hU^{*2}}{2\nu}, & 0 \leqslant h < \delta, \\ \frac{\delta^2 U^{*2}}{2h\nu} + \frac{U^*}{k}\left[\ln\frac{hU^*}{\nu} + kC - 1 - \frac{B\delta}{h}\right], & \delta \leqslant h < \frac{H}{2}, \\ \frac{\delta^2 U^{*2}}{2h\nu} + \frac{HU^*}{hk}\ln\frac{H}{4(H-h)} + \frac{U^*}{k}\left[\ln\frac{(H-h)U^*}{\nu} + kC - 1 - \frac{B\delta}{h}\right], & \frac{H}{2} \leqslant h < H-\delta, \\ \frac{[(H-h)^2+2\delta^2]U^{*2}}{2h\nu} + \frac{HU^*}{hk}\ln\frac{H}{2\delta} + \frac{B(H-2\delta)U^*}{hk}, & H-\delta \leqslant h \leqslant H. \end{cases} \tag{5}$$

Here, B is

$$B = \ln\frac{\delta U^*}{\nu} + kC - 1. \tag{6}$$

Combining Eqs. (3)–(6) yields the relationship between $\overline{U}_h$ and $\overline{U}_H$. Practically, $\overline{U}_H$ can be measured, but $\overline{U}_h$ can form a Reynolds number to quantify the gas shearing effect on a droplet.

For a stable and deformed droplet, contact angles are different along the three-phase contact lines. Advancing contact angle θ_a and receding contact angle θ_r are only called at the beginning of droplet motion. Fig. 2b shows a deformed droplet, coming from an equivalent droplet without deformation shown in Fig. 2c. The equivalent droplet is above on the wall without gas shearing, it is useful to obtain geometry parameters for deformed droplet. Both deformed droplet and equivalent droplet have the same volume V:

$$V = \frac{\pi}{3}r^3(2 - 3\cos\theta_e + \cos^3\theta_e). \tag{7}$$

The contact area between droplet and solid wall, A_a, is

$$A_a = \pi r^2 \sin^2\theta_e. \tag{8}$$

The upwind project area of the droplet in the gas stream, E_d, is

$$E_d = \frac{2\theta_e - \sin(2\theta_e)}{2}r^2. \tag{9}$$

The droplet height h is

$$h = r(1 - \cos\theta_e). \tag{10}$$

Eqs. (7)–(10) show that all the droplet geometry parameters are defined using droplet radius r and equilibrium contact angle CA, θ_e.

3. Critical criterion equation and results for droplet sliding

3.1. Critical criterion equation for droplet sliding

Fig. 3 shows the force balance. For droplet sliding, shear force and gravity force are the driving force, but surface tension resists droplet motion. At the onset of sliding, forces in the x-direction (parallel to the wall) are of interest. In fact, surface tension force is an integration effect along the foot print contact lines. It is necessary to determine the contact angles at different

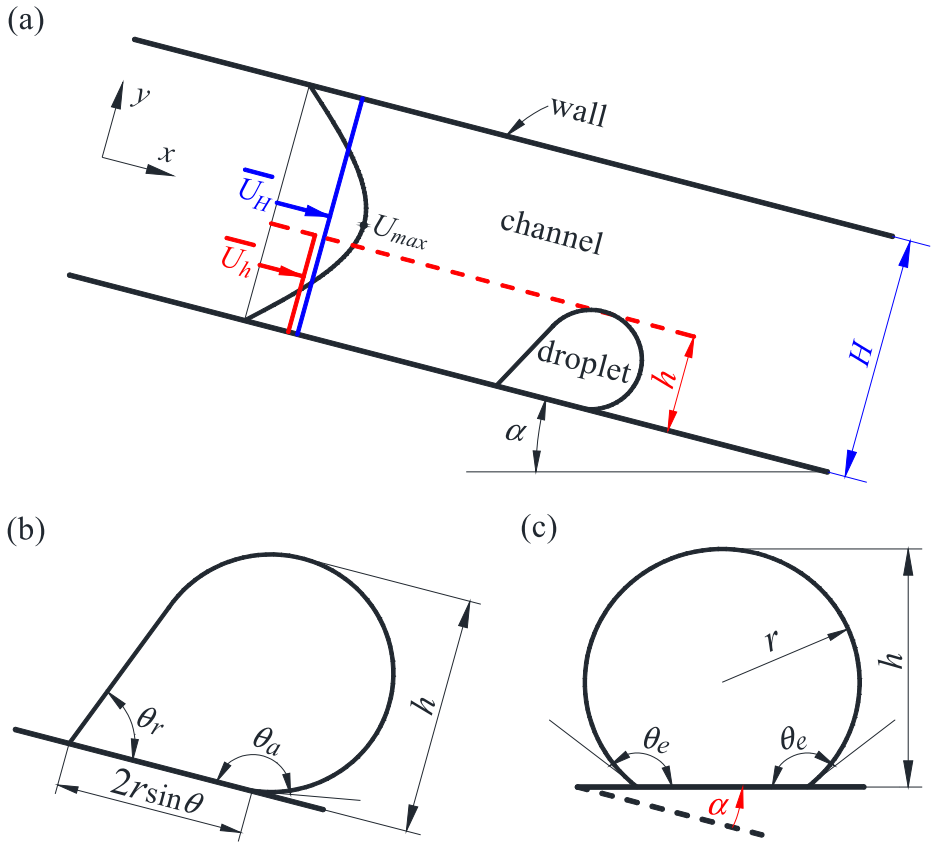

Fig. 2. Physical model and parameters definition for droplet sliding.

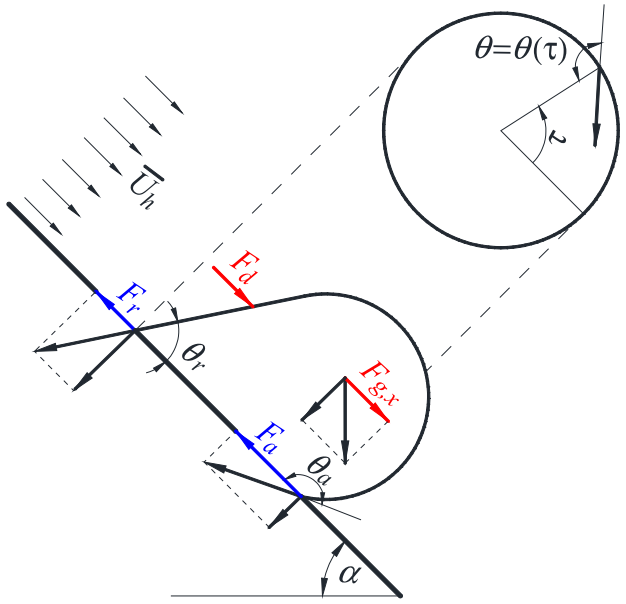

Fig. 3. Force balance for onset of droplet sliding.

locations along the circular contact lines. Contact angle hysteresis, namely, the variation between advancing and receding contact angle, is assumed to have linear distribution versus azimuthal angle τ [18]:

$$\cos\theta = \cos\theta_a + \left(\frac{\cos\theta_r - \cos\theta_a}{\pi}\right)\tau. \tag{11}$$

The net surface tension force in x component is

$$F_{\sigma,x} = 2r\sigma\sin\theta_e\int_0^{\pi}\cos\theta\cos\tau\,d\tau = -\frac{4}{\pi}r\sigma\sin\theta_e(\cos\theta_r - \cos\theta_a), \tag{12}$$

where σ is the surface tension between gas and liquid.

As a driving force, gravity force in x component is

$$F_{g,x} = \frac{\pi}{3}r^3(2 - 3\cos\theta_e + \cos^3\theta_e)(\rho_l - \rho_g)g\sin\alpha, \tag{13}$$

where ρ is the density, g is the gravity acceleration. The subscripts l and g represent liquid and gas. The shear force in x component is another driving force, which is [24]:

$$F_d = \frac{1}{2}\rho_g U^2 C_d E_d, \tag{14}$$

where C_d is drag coefficient, U is characteristic gas velocity, which can be $\overline{U}_h$ defined in Section 2.

Fewer studies dealt with C_d for liquid droplet in gas flow. Suh and Lee [25] showed that liquid droplet and solid particle have similar drag coefficients. For a solid particle in a uniform gas velocity field, the Stokes drag force is

$$F_d = 6\pi\mu rU = \frac{1}{2}\rho_g U^2 \times \frac{24}{Re_D} \times \pi r^2, \tag{15}$$

where $C_d = 24/Re_D$ is called the Stokes drag coefficient, which is suitable for sphere particle sheared by uniform gas stream without flow boundary separation and $Re < 0.4$. Many investigators modified C_d for extending application range of Re. We choice the following expression listed as one of the widely used expression to estimate drag coefficients by Ceylan et al. [26]:

$$C_d = \left(0.352 + \sqrt{0.124 + \frac{24}{Re_h}}\right)^2. \quad (16)$$

Eq. (16) has been verified by large quantity of experimental data and is suitable for $0.1 < Re < 10^4$ [27]. In order to adapt the spherical crown shape droplet, the droplet height $h = r(1 - \cos\theta_e)$ characterizes the Reynolds number:

$$Re_h = \frac{\rho_g h \overline{U}_h}{\mu_g} = \frac{\rho_g r \overline{U}_h}{\mu_g}(1 - \cos\theta_e) = Re(1 - \cos\theta_e), \quad (17)$$

where μ_g is the gas viscosity. We note that Re and Re_h are characterized by the droplet radius r and droplet height h, respectively. Holding Eqs. (16) and (17), Eq. (15) becomes

$$F_d = \frac{1}{2}\rho_g \overline{U}_h^2 C_d E_d = \frac{2\theta_e - \sin(2\theta_e)}{4} C_d r^2 \rho_g \overline{U}_h^2. \quad (18)$$

Up to now, the force balance principle writes

$$F_{g,x} + F_d + F_{\sigma,x} = 0. \quad (19)$$

Substituting Eqs. (12), (13) and (18) into Eq. (19) yields the following non-dimensional equation:

$$\frac{\pi}{6}\sin\alpha Bn + \frac{\psi_1}{8} C_d We - \Gamma_1 = 0, \quad (20)$$

where We is the Weber number, characterizing relative importance of inertia force related to surface tension force:

$$We = \frac{\rho_g r \overline{U}_h^2}{\sigma}. \quad (21)$$

Bn is the Bond number, representing the competition between buoyancy force and surface tension force. Because ρ_g is much smaller than ρ_l, it can also say that Bn represents the competition between liquid gravity and surface tension force. Bn, Ψ_1 and Γ_1 are

$$Bn = \frac{(\rho_l - \rho_g) g r^2}{\sigma}, \quad (22)$$

$$\psi_1 = \frac{2\theta_e - \sin(2\theta_e)}{(1 - \cos\theta_e)^2(2 + \cos\theta_e)}, \quad (23)$$

$$\Gamma_1 = \frac{2\sin\theta_e(\cos\theta_r - \cos\theta_a)}{\pi(1 - \cos\theta_e)^2(2 + \cos\theta_e)}. \quad (24)$$

It is noted that previous studies [5,12,24,28] dealt with either gravity force, or shear force, to be competed against surface tension force. Eq. (20) is our newly developed criterion equation for onset of droplet sliding, which is a *hybrid non-dimensional force balance equation*, comprehensively reflecting relative importance of various factors on droplet sliding. Eqs. (20)–(24) show that critical condition for droplet sliding depends on three groups of parameters: (1) non-dimensional competition force parameters of Bn, We and Re, where Re determines C_d; (2) inclination angle parameter of $\sin\alpha$; and (3) wettability parameters of Ψ_1 and Γ_1, where Ψ_1 is only related to θ_e. Contact angle hysteresis number is defined as $\Omega = \cos\theta_r - \cos\theta_a$. Thus, Γ_1 is related to θ_e and Ω. Eq. (20) has three functions:

(1) *To predict the "sliding angle":* "Rolling angle" widely appeared in the literature means the smallest inclination angle at which a droplet begins to move, meaning "detachment" only. The "detachment mode" (for example, sliding or rolling) is not identified. Thus, we propose a new term of "sliding angle" as the smallest inclination angle at which a droplet begins to slide on the wall. The sliding angle induced by Eq. (20) is

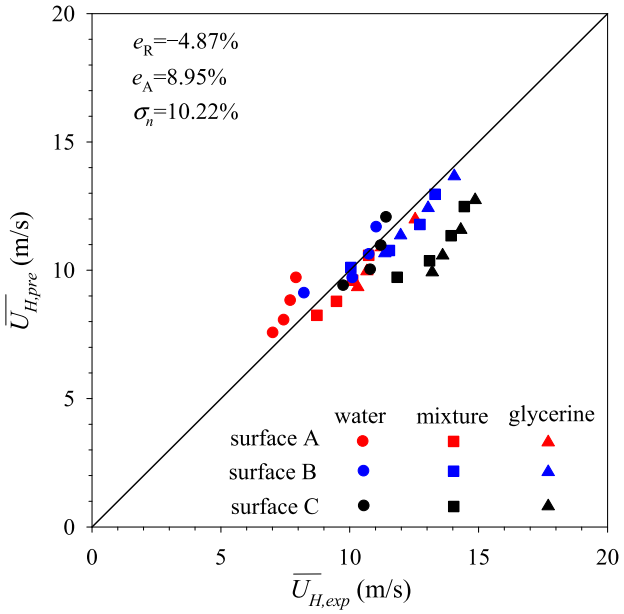

Fig. 4. Comparisons of measured and predicted average gas velocity over the whole channel height H at the critical condition ($\overline{U}_{H,exp}$ is the measured value from Fan et al. [11], $\overline{U}_{H,pre}$ is the predicted value, linking $\overline{U}_{h,cr}$ by Eqs. (3)–(6), where $\overline{U}_{h,cr}$ is the average gas velocity over the droplet height h and it is determined by Eq. (20)).

$$\alpha_{\text{"sliding angle"}} = \arcsin\left(\frac{24\Gamma_1 - 3\psi_1 C_d We}{4\pi Bn}\right). \quad (25)$$

(2) *To predict the critical gas velocity:* A droplet is stable on the wall, until it begins to slide at a critical gas stream velocity $\overline{U}_{h,cr}$. Replacing $\overline{U}_h$ by $\overline{U}_{h,cr}$ and substituting $\overline{U}_{h,cr}$ into Re in Eq. (17) and We in Eq. (21), Eq. (20) forms a transcendental equation $f(\overline{U}_{h,cr}) = 0$, which can be iteratively solved to obtain $\overline{U}_{h,cr}$.

(3) *To predict* r_{max}: r_{max} specifies the maximum droplet size that can stay on a wall, beyond which the droplet begins to slide. Substituting r_{max} into Re, We and Bn, Eq. (20) forms a transcendental equation $f(r_{max}) = 0$, which can be iteratively solved to obtain r_{max}. At the zero shear force, Eq. (20) has a particular solution:

$$r_{max} = \sqrt{\frac{12}{\pi^2} \times \frac{\sin\theta_e(\cos\theta_r - \cos\theta_a)}{(2 - 3\cos\theta_e + \cos^3\theta_e)} \times \frac{\sigma}{(\rho_l - \rho_g) g \sin\alpha}}. \quad (26)$$

Our developed particular solution in Eq. (26) is almost identical to that given by Sikarwar et al. [29]. The coefficient of $12/\pi^2 = 1.22$ in Eq. (26) approaches the value of 1.25 given by Sikarwar et al. [29].

3.2. Comparison with measurements

Fan et al. [11] examined onset of droplet motion through a shearing mechanism generated by a controlled air flow. A droplet was placed on the bottom wall in a wind channel of 80 mm width, 20 mm height and 200 mm length. Experiments were performed over a range of fluids and well defined surfaces. Droplet fluids were water, pure glycerine and water-glycerine mixture (1:1 vol ratio), respectively. The bottom wall was treated by n-hexyltrimethoxysilane (surface A), methyltrimethoxysilane (surface B) and n-octyltriethoxysilane (surface C), respectively. The wind channel was horizontally positioned. Physical properties

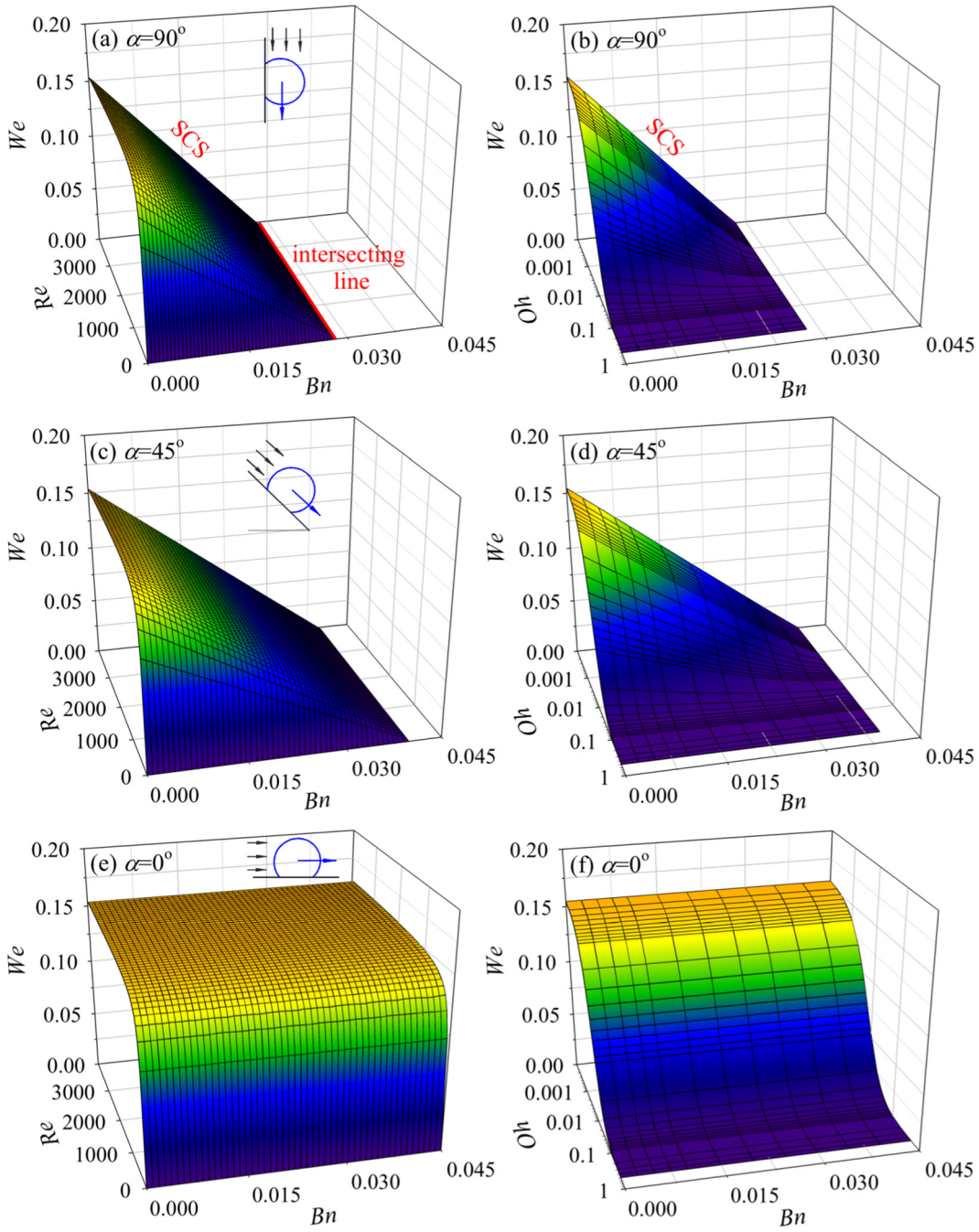

Fig. 5. Effect of α on sliding criterion surfaces ($\theta_e = 135°$ and $\Omega = \cos\theta_r - \cos\theta_a = 0.123$).

of air are $\rho_g = 1.205$ kg/m^3 and $\mu_g = 17.9 \times 10^{-6}$ Pa s. The iterative solution of Eq. (20) yields critical air velocity $\overline{U}_{h,cr}$. Then, the average gas velocity over the whole channel height $\overline{U}_{H,cr}$ at the critical condition is linked to $\overline{U}_{h,cr}$ using Eqs. (3)–(6). $\overline{U}_{H,cr}$ is recorded as $\overline{U}_{H,pre}$ for our predictions and $\overline{U}_{H,exp}$ for Fan et al. [11] experimental data. Fig. 4 shows the direct comparison. The definition of average deviation e_R, mean absolute deviation e_A and standard deviation σ_n can be found in Ref. [30], where e is called deviation, n is the number of data points (here $n = 36$). These parameters quantify the matching degree between predictions and measurements. It is shown that e_R, e_A and σ_n are 4.87%, 8.95% and 10.22%, respectively. The matching is excellent.

3.3. Effect of various parameters on droplet sliding

Once *Re* and *We* are given, the Ohnesorge number (*Oh*) can be determined as [31]:

$$Oh = \frac{\sqrt{We}}{Re} = \frac{\mu_g}{\sqrt{\rho_g \sigma r}}. \tag{27}$$

An alternative way to present the relationship among *Bn*, *Re* and *We* is to present the relationship between *Bn*, *Oh* and *We*. For the latter presentation, the gas velocity only influences *We* but not influences *Oh*. For general consideration, suitable *Bn* and *Oh* ranges should be determined. *We* is treated as the dependent variable to

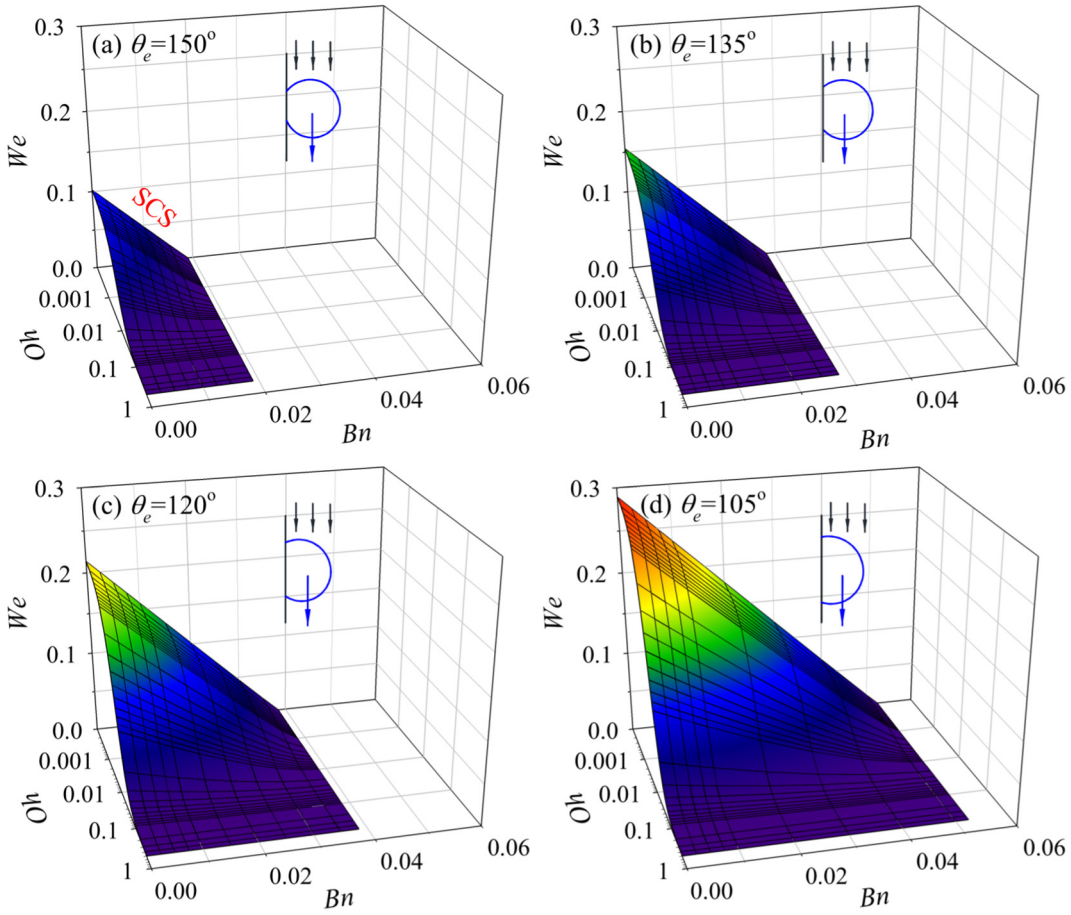

Fig. 6. Effect of θ_e on sliding criterion surface ($\alpha = 90°$ and $\Omega = \cos\theta_r - \cos\theta_a = 0.123$).

be solved by Eq. (20) with *Bn* and *Oh* as independent variables. A wide range of two-phase fluids (52 gases and 64 liquids) are considered, whose physical properties come from Ref. [32]. These fluids are frequently encountered in nature and engineering. Gases include air containing different species and various organic fluid vapors. Liquids include organic liquids, water, bromium and metal liquids such as mercury (Hg). For the estimation of *Bn* and *Oh* ranges, droplet radius had the range of $r = 1\ \mu m - 1$ mm. The orthogonality combination of physical properties of the two fluids and droplet radius results in $Oh = 0.18 \times 10^{-3} - 0.49$, in which 0.18×10^{-3} is obtained for RC318 (organic fluid) vapor shearing a 1 mm radius Hg droplet, and 0.49 is reached for helium gas shearing a 1 μm radius perflenapent droplet. Similarly, Bond number had the range of $Bn = 2.8 \times 10^{-8} - 1.57$. Figs. 5–7 yield the following findings:

3.3.1. Relationship among Bn, Oh and We

At fixed α, Ψ_1 and Γ_1, Fig. 5 shows sliding criterion surface (SCS) of *Bn*, *Re* and *We*, and of *Bn*, *Oh* and *We*, above which a droplet slides and below which a droplet is stable. *We* are increased with increases of *Re*, but decreased with increases of *Bn*. Besides, *We* are decreased with increases of *Oh*. Physically, SCS indicates the contributions of shear force, gravity force and surface tension force on the onset of droplet sliding.

3.3.2. Effect of inclination angles

Inclination angle influences gravity component parallel to the wall to influence droplet sliding. Fig. 5 shows the largest sliding region at vertical position ($\alpha = 90°$) and smallest sliding region at horizontal position ($\alpha = 0°$). The latter makes no gravity contribution to the droplet sliding. The decreased inclination angles narrows the sliding region. The criterion surface intersects $We = 0$ plane to form a intersecting line, representing zero shear force condition. The line is $Bn = 0.028$ at $\alpha = 90°$ but becomes 0.040 at $\alpha = 45°$. SCS does not intersect $We = 0$ plane at $\alpha = 0°$, because a droplet cannot slide at zero shear force without gravity contribution.

3.3.3. Effect of equilibrium contact angles

Fig. 6 shows the shrinking of droplet sliding region by decreasing equilibrium contact angle (CA) of θ_e, keeping the constant $\cos\theta_r - \cos\theta_a = 0.123$.

3.3.4. Effect of contact angle hysteresis

The larger the Ω, the larger deformation of a droplet is. Fig. 7 shows that the CA hysteresis effect is strong. The sliding region becomes smaller by gradual increasing CA hysteresis number Ω from sub-figure *a* to *d*. A "rigid" droplet is easy to slide but a "soft" droplet is difficult to slide.

4. Critical criterion equation and results for droplet rolling

4.1. Critical criterion equation for droplet rolling

Now we turn to determine the onset of droplet rolling. Fig. 8 shows the physical model for torque analysis to initiate rolling.

The three-phase contact point O is the pivot point. L_d is the moment arm for shear force F_d. L_g is the moment arm for x-component gravity force $F_{g,x}$, which is also the distance from the center of droplet mass to the solid wall:

$$L_g = \frac{3 - 2\cos\theta_e - \cos^2\theta_e}{8 + 4\cos\theta_e} r. \tag{28}$$

The gravity force torque T_g is

$$T_g = F_{g,x} L_g = \frac{\pi}{12}(3 - 8\cos\theta_e + 6\cos^2\theta_e - \cos^4\theta_e)(\rho_l - \rho_g) g r^4 \sin\alpha. \tag{29}$$

Shear force is equivalent to act on a specific point, from which to the solid wall is L_d:

$$L_d = \int_0^{\theta_e} r(\cos\beta - \cos\theta_e)\sin\beta d\beta. \tag{30}$$

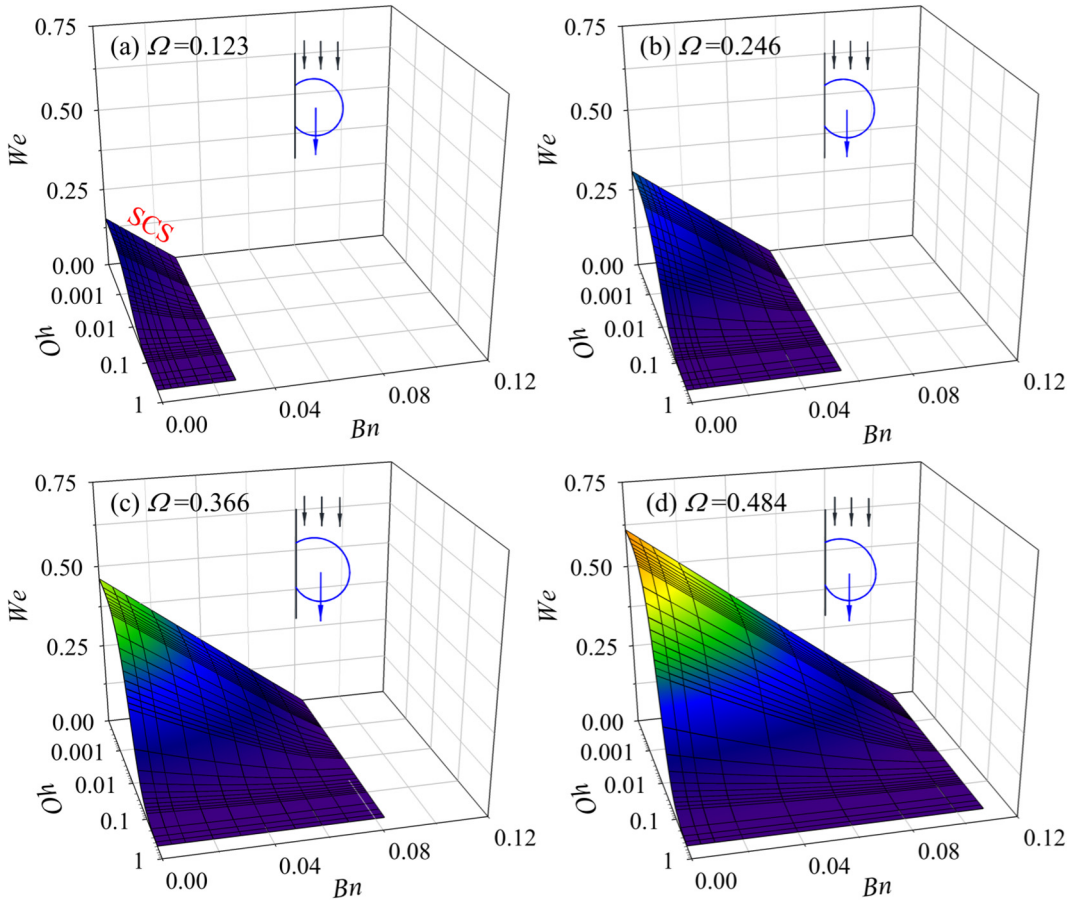

Fig. 7. Effect of Ω on sliding criterion surface ($\alpha = 90°$ and $\theta_e = 135°$).

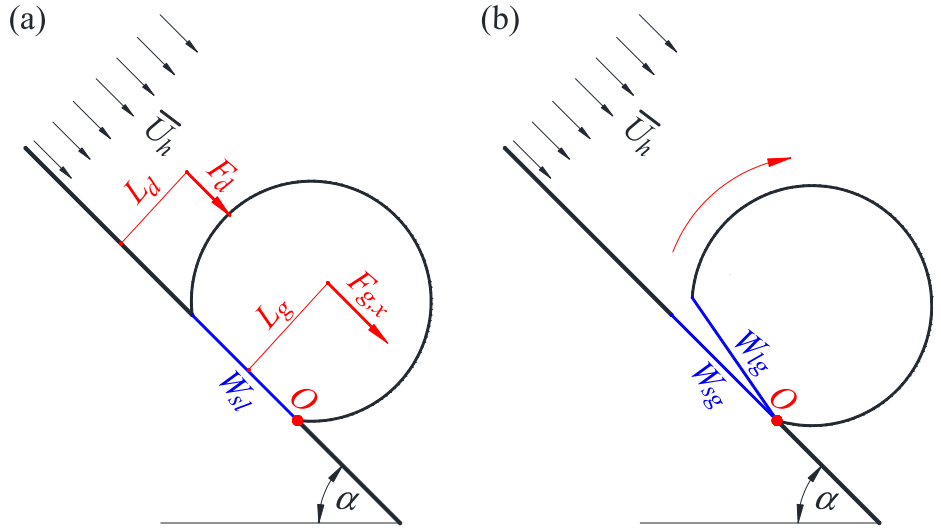

Fig. 8. Torque balance for onset of droplet rolling.

Combining Eqs. (18) and (30) yields the shear force torque as

$$T_d = F_d L_d = \frac{2\theta_e - \sin(2\theta_e)}{8}(1-\cos\theta_e)^2 \rho_g r^3 C_d \overline{U}_h^2. \quad (31)$$

Before droplet rolling, droplet footprint on the wall is the solid-liquid interface, represented by "*sl*" (see Fig. 8a). Once the droplet rolls, the solid-liquid interface on the wall is replaced by the solid-gas interface, represented by "*sg*", and the liquid-gas interface on the droplet, represented by "*lg*" (see Fig. 8b). Adhesion work is the difference of surface energy before and after the droplet rolls. Again, local contact angles are changed between the advancing contact angle and receding contact angle, and are assumed to have linear distribution versus azimuthal angle τ. Then, adhesion work is

$$W = \int_0^{\pi} \pi\sigma r^2 (1+\cos\theta)\sin^2\theta_e \cos\tau d\tau = -2\sin^2\theta_e(\cos\theta_r - \cos\theta_a)\sigma r^2. \quad (32)$$

The torque balance principle yields

$$T_g + T_d + W = 0. \quad (33)$$

Substituting Eqs. (29), (31) and (32) into Eq. (33) reaches

$$\frac{\pi}{12} Bn \sin\alpha + \frac{\psi_2}{8} C_d We - \Gamma_2 = 0, \quad (34)$$

where Ψ_2 and Γ_2 are as follows

$$\psi_2 = \frac{2\theta_e - \sin(2\theta_e)}{(1-\cos\theta_e)(3+\cos\theta_e)}, \quad (35)$$

$$\Gamma_2 = \frac{2(1+\cos\theta_e)(\cos\theta_r - \cos\theta_a)}{(1-\cos\theta_e)^2(3+\cos\theta_e)}. \quad (36)$$

Eq. (34) is our newly developed hybrid non-dimensional torque balance equation for onset of droplet rolling, having three functions:

(1) *To predict the "rolling angle":* Here, "rolling angle" is defined as the smallest inclination angle at which a droplet begins to roll on the wall, which is predicted by Eq. (34) as

$$\alpha_{\text{"rolling angle"}} = \arcsin\left(\frac{24\Gamma_2 - 3\psi_2 C_d We}{2\pi Bn}\right). \quad (37)$$

We note that "rolling angle" in this paper is specifically for rolling motion, but "rolling angle" in the literature is a general term, not considering the detachment mode.

(2) *To predict the critical gas velocity:* Substituting critical gas velocity $\overline{U}_{h,cr}$ into Eq. (34), a transcendental equation $f(\overline{U}_{h,cr}=0)$ is formed, which can be iteratively solved to obtain $\overline{U}_{h,cr}$ for the onset of droplet rolling.

(3) *To predict r_{max}*: Substituting r_{max} into *Re*, *We* and *Bn* of Eq. (34), a transcendental equation $f(r_{max}) = 0$ is formed, which can be iteratively solved to obtain r_{max} for the onset of droplet rolling. At the zero shear force, Eq. (34) has a particular solution:

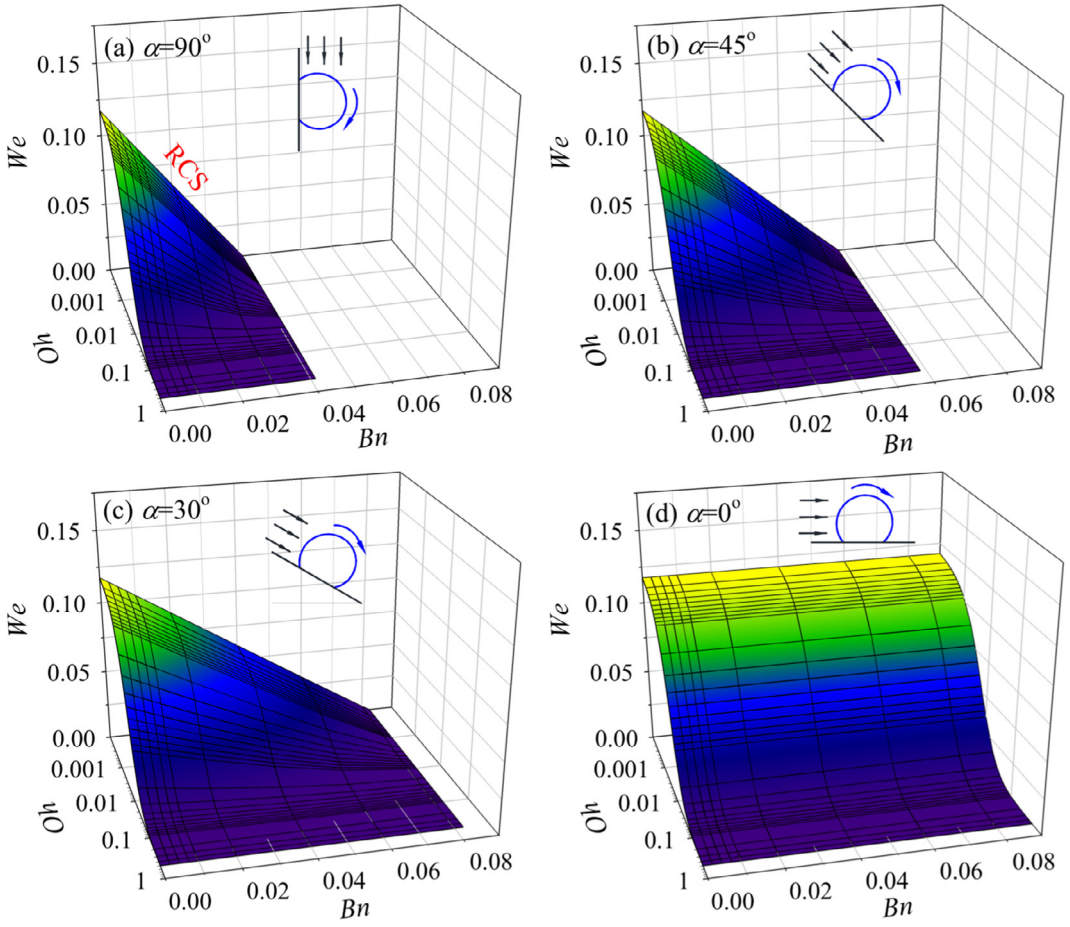

Fig. 9. Effect of α on rolling criterion surfaces (θ_e = 135° and $\Omega = \cos\theta_r - \cos\theta_a$ = 0.123).

$$r_{max} = \sqrt{\frac{24}{\pi} \times \frac{(1+\cos\theta_e)(\cos\theta_r - \cos\theta_a)}{3 - 5\cos\theta_e + \cos^2\theta_e + \cos^3\theta_e} \times \frac{\sigma}{(\rho_l - \rho_g) g \sin\alpha}}. \quad (38)$$

4.2. Effect of various parameters on droplet rolling

Figs. 9–11 plot three-dimensional rolling criterion surface (RCS), above which a droplet rolls, and below which a droplet is stable.

4.2.1. Effect of inclination angles

The vertical wall ($\alpha = 90°$) has the largest rolling region. Decrease of inclination angles makes difficult to rotate a droplet on the wall, due to the decreased gravity force torque. At the same *We*, *Bn* is increased for smaller α (see Fig. 9).

4.2.2. Effect of equilibrium contact angles

Fig. 10a shows that a droplet is very easy to roll on the wall at an equilibrium *CA* of 150°, which is consistent with our common knowledge. The rolling region is apparently decreased when *CA* is decreased (see sub-figure *a* to *d* in Fig. 10).

4.2.3. Effect of contact angle hysteresis

CA hysteresis significantly influences rolling criterion. Smaller CA hysteresis such as $\Omega = 0.123$ results in larger rolling region. A "rigid" droplet is easy to roll but a "soft" droplet is difficult to roll (see Fig. 11).

5. Transition criterion between sliding and rolling modes

Comparison of Figs. 5–7 and 9–11 indicates that *Bn*, *Oh* and *We* are in the same magnitudes for droplet sliding and rolling. Eqs. (20) and (34) are independently developed for the two detachment modes. One may ask a question: which mode does a droplet prefer if a droplet can move, sliding or rolling? Thus, the transition between sliding and rolling should be analyzed.

We remember that four droplet removal modes are mentioned in Introduction. Practically, lifting and dripping are difficult to happen in nature and engineering. Fig. 12 shows the force analysis for lifting motion. Because lifting occurs in the direction perpendicular to the wall, lifting force F_l is the driving force:

$$F_l = \frac{1}{2}\rho_g \overline{U}_h^2 C_l \pi r^2, \quad (39)$$

where C_l is the lifting force coefficient. The ratio of η is defined as the lifting force divided by the drag force. Combining Eqs. (18) and (39) yields

$$\eta = \frac{F_l}{F_d} = \frac{2\pi}{2\theta_e - \sin(2\theta_e)} \frac{C_l}{C_d}. \quad (40)$$

A hydrophobic surface ($\theta_e > 90°$) results in $1 < \frac{2\pi}{2\theta_e - \sin(2\theta_e)} < 2$. C_l is one to two orders smaller than C_d [33], causing η much smaller than 1 ($\eta << 1$), explaining why a droplet is more difficult to be lifting, compared with sliding or rolling. Dripping is also very strict to occur, except that when the droplet is underneath a

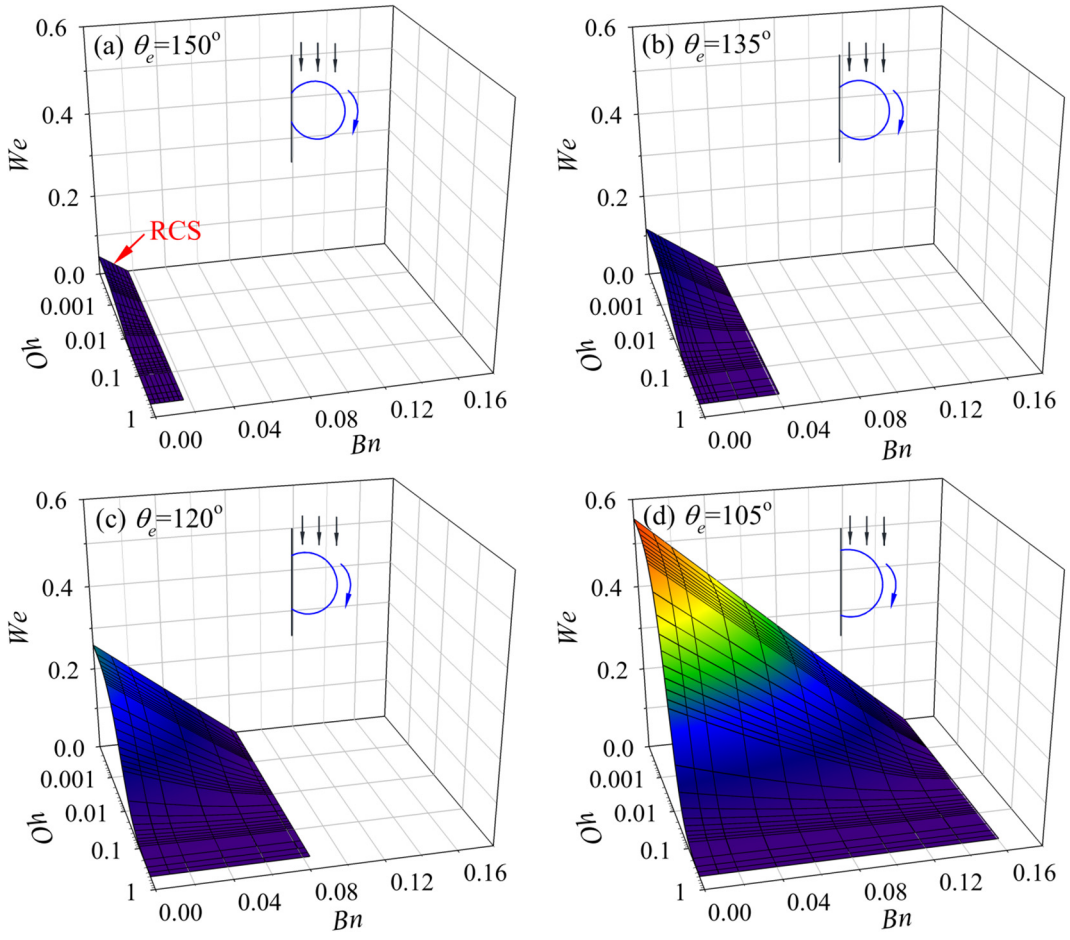

Fig. 10. Effect of θ_e on rolling criterion surface ($\alpha = 90°$ and $\Omega = \cos\theta_r - \cos\theta_a = 0.123$).

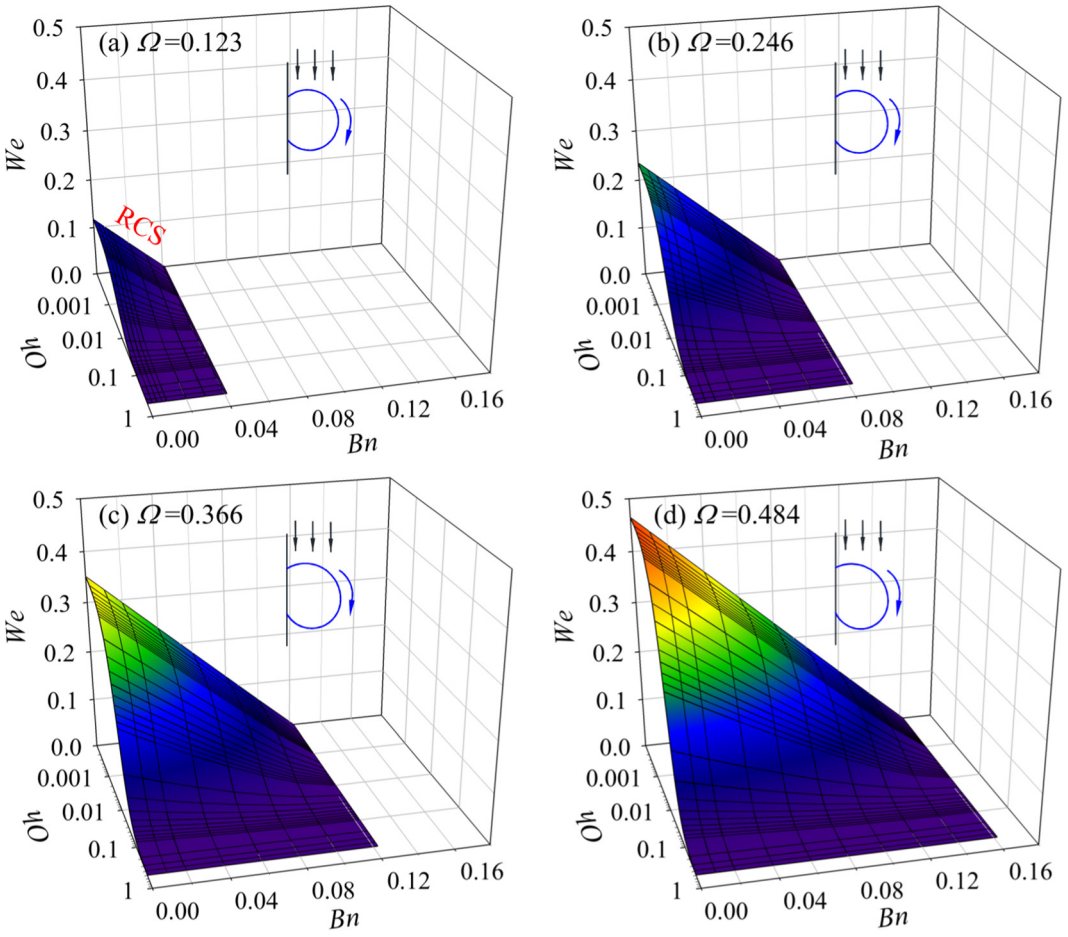

Fig. 11. Effect of Ω on rolling criterion surface ($\alpha = 90°$ and $\theta_e = 135°$).

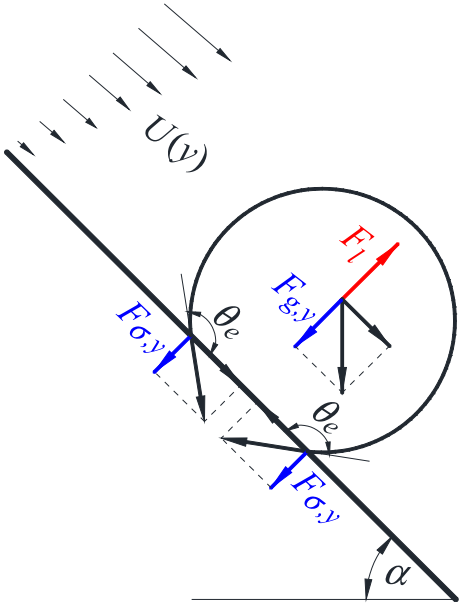

Fig. 12. Force balance for onset of droplet lifting.

quasi-horizontal wall. Thus, we only develop the transition criterion between sliding and rolling. Linking Eq. (20) for sliding and Eq. (34) for rolling gets

$$Bn_t \sin\alpha = \frac{12}{\pi}\frac{\Gamma_1\psi_2 - \Gamma_2\psi_1}{2\psi_2 - \psi_1} = \frac{24}{\pi^2}\frac{(\cos\theta_r - \cos\theta_a)[\sin\theta_e(1-\cos\theta_e) - \pi(1+\cos\theta_e)]}{(1-\cos\theta_e)^2(1-3\cos\theta_e - 2\cos^2\theta_e)}. \quad (41)$$

The right side of Eq. (41) is dependent on equilibrium contact angle θ_e and contact angle hysteresis parameter $\Omega = \cos\theta_r - \cos\theta_a$. Eq. (41) is called the transition criterion equation between sliding and rolling.

In Fig. 13, sliding criterion surface (SCS) and rolling criterion surface (RCS) are represented by blue color and black color, respectively. Eq. (41) determines a specific transition Bond number Bn_t once α, θ_e and Ω are given. In the left of Bn_t line, $Bn < Bn_t$, RCS is under SCS to mean that rolling is easier to happen than sliding, yielding rolling mode. On the other hand, in the right of Bn_t line, $Bn > Bn_t$, SCS is under RCS to choose sliding mode.

In Fig. 13b, a cross section of $Oh = 0.001$ was chosen to present sliding criterion curve (SCC) and rolling criterion curve (RCC). A droplet selects mode according to practical criterion curve (PCC represented by solid curve), consisting of a rolling part ahead of the transition point, and a sliding part beyond the transition point. Fig. 13c shows the practical criterion surface, including a rolling part and a sliding part, interfaced by the Bn_t line. Fig. 13c is also called the mode selection surface here. Bn_{max} is the maximum Bond number, which is the intersecting line between SCS and the $We = 0$ plane.

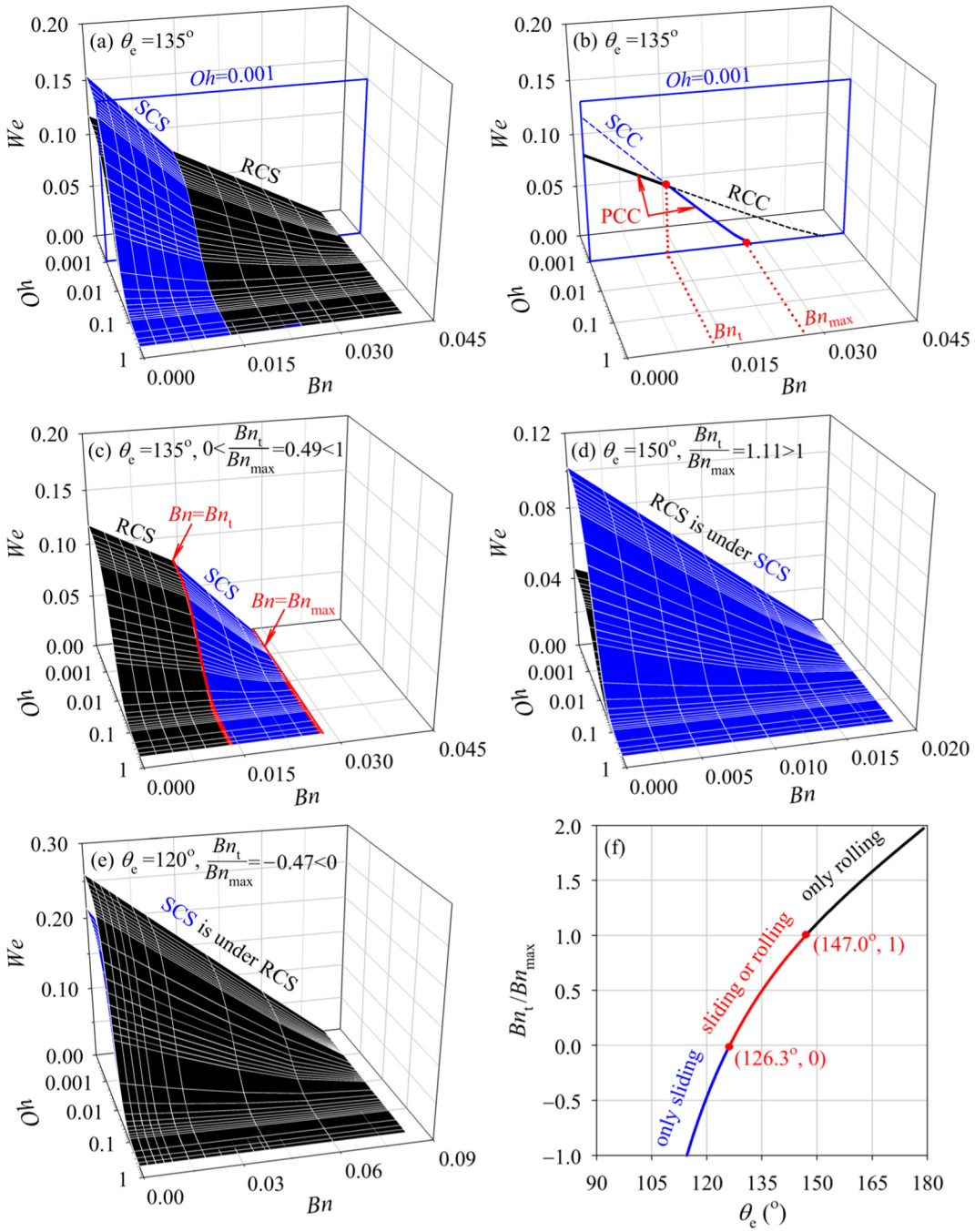

Fig. 13. Mode selection between sliding and rolling ($\alpha = 90°$ and $\Omega = \cos\theta_r - \cos\theta_a = 0.123$ for sub-figures a–e, sub-figure f for Bn_t/Bn_{max} versus θ_e).

Fig. 13a–c indicates the mode selection dependent on Bn_t location related to Bn_{max}. SCS and RCS do intersect for the range of $0 < Bn_t/Bn_{max} < 1$. If Bn_t shifts to left, the RCS region is contracted but the SCS region is enlarged. Alternatively, if Bn_t shifts to right, the RCS region is enlarged but the SCS region is contracted. Thus, the parameter of Bn_t/Bn_{max} is introduced to quantify the mode selection between sliding and rolling. Bn_{max} is deduced by Eq. (20) as

$$Bn_{max}\sin\alpha = \frac{6}{\pi}\Gamma_1 = \frac{12}{\pi^2}\frac{\sin\theta_e(\cos\theta_r - \cos\theta_a)}{(1-\cos\theta_e)^2(2+\cos\theta_e)}. \quad (42)$$

Combining Eqs. (41) and (42) yields

$$\frac{Bn_t}{Bn_{max}} = f(\theta_e) = \frac{(4+2\cos\theta_e)[\sin\theta_e(1-\cos\theta_e) - \pi(1+\cos\theta_e)]}{\sin\theta_e(1-3\cos\theta_e - 2\cos^2\theta_e)}. \quad (43)$$

Eq. (43) is called the mode selection criterion equation, which is only relied on the equilibrium contact angles. The contact angle hysteresis parameter Ω influences both Bn_t and Bn_{max}, but it does not influence Bn_t/Bn_{max}, representing the ratio of RCS project area to the total project areas of RCS and SCS on the $We = 0$ plane. The solution of $f(\theta_e) = 0$ and $f(\theta_e) = 1$ correspond to $\theta_e = 126.3°$ and $\theta_e = 147.0°$, respectively. Three regions are as follows:

Region 1 ($126.3° < \theta_e < 147.0°$): The range of $126.3° < \theta_e < 147.0°$ yields $0 < f(\theta_e) < 1$. Practical mode consists of a rolling part ahead of Bn_t and a sliding part beyond Bn_t. In other words, *a droplet prefers to roll if $Bn < Bn_t$, and prefers to slide if $Bn > Bn_t$* (see Fig. 13a–c).

Region 2 ($\theta_e > 147.0°$): For $We > 0$ and $\theta_e > 147.0°$, $f(\theta_e) > 1$ means no intersection of RCS and SCS. RCS is under SCS to yield rolling mode only (see Fig. 13d). The 147.0° contact angle theoretically developed in this paper is recommended as the new contact angle boundary for wettability transition from hydrophobicity to super-hydrophobicity. The 147.0° CA approaches the widely used 150° for our common knowledge.

Region 3 ($\theta_e < 126.3°$): For $We > 0$ and $\theta_e < 126.3°$, $f(\theta_e) < 0$ means no intersection of SCS and RCS. SCS is under RCS to choose sliding mode only (see Fig. 13e).

Fig. 13f summarized the mode selection dependent on equilibrium contact angles according to Eq. (43). Both equilibrium contact angle and contact angle hysteresis determine if a droplet can be initiated to slide or roll. But the mode selection is determined by equilibrium contact angles only, once the drop motion can be initiated.

6. Comparison with other works

Our work is different from previous studies in three aspects. First, our critical criterion equations and mode selection criterion equation are in non-dimensional form and contain no empirical coefficient. These equations can be applied to various working fluids, channel sizes and gas velocities, etc. Experimental studies such as Fan et al. [11], Polverino et al. [22] and Fu et al. [23], as well as numerical simulations such as Cho et al. [10] and Theodorakakos et al. [6] are for specific test section arrangement, gas-liquid fluids and droplet sizes. These studies enhance the understanding of droplet motion. However, the results are difficult to be extended from a general sense. Second, our study treats the comprehensive competition between surface tension force, gravity force and shear force. The comprehensive effects are not reported in the literature. For example, Chen [9] and Cho et al. [10] just treated sliding under the effects of shear force and surface tension force. Dimitrakopoulos and Higdon [12] tackled sliding with surface tension force competed by gravity force. The maximum droplet radius obtained by Sikarwar et al. [28] is one of our particular solutions for sliding. Lastly, our significant contribution is highlighted on the coupling of the two criterion equations for sliding and rolling to determine the specific mode, enhancing the understanding of droplet dynamics on surfaces with different wettabilities. Previous studies investigated either the sliding motion [9–12], or the rolling motion [18,19]. Fewer authors investigated two detachment modes such as Sikarwar et al. [7,29] for sliding and dripping, and Basu et al. [20] for sliding and lifting. But the coupling of different motion modes is not reported.

Our theoretical work assumes that the droplet footprint has circular shape. Such an assumption is also used in Refs. [5,9,21]. Under specific conditions, the droplet footprint may slightly deviate from a circular shape [34]. We note that there are no experimental data for onset of rolling in the literature. More experiments are recommended to support the newly developed theory in this paper, especially for onset of rolling and mode selection between sliding and rolling. Data should be provided including equilibrium contact angle, contact angle hysteresis and gas velocity, etc.

7. Conclusions

Droplet detachment widely occurs in nature and engineering facilities. For such a problem, two questions should be answered: (1) at what condition a droplet begins to move? (2) what is the motion mode if a droplet can move? Here, we deal with a general problem having a wall contacted droplet sheared by a gas stream. For two common motion modes of sliding and rolling, we developed two critical criterion equations independently, considering the surface tension force, gravity force and shear force. Both criterion equations are written using dimensionless parameters which reflect relative contributions of various factors on droplet instability induced by sliding or rolling. The two equations can predict critical gas velocity, inclination angle and maximum droplet size at the onset of sliding or rolling, separately.

To resolve the second question, the two critical criterion equations of sliding and rolling are coupled to develop a mode selection criterion equation, for the first time. Coupling of the two motion modes results in new understanding of droplet detachment. We show that both equilibrium contact angle and contact angle hysteresis influence if sliding or rolling can happen, but the mode selection is only dependent on equilibrium contact angle if sliding or rolling are sure to occur. The mode selection is found to have three regions: $\theta_e > 147.0°$ for rolling only, $\theta_e < 126.3°$ for sliding only, and $126.3° < \theta_e < 147.0°$ for pending mode depending on Bond number. The 147.0° contact angle is suggested as the new boundary for wettability transition from hydrophobicity to super-hydrophobicity.

Conflict of interest

The authors declared that there is no conflict of interest.

Acknowledgements

The authors thanks for the funding support by National Natural Science Foundation of China (51436004) and 111 Project (B12034).

Appendix A. Supplementary material

Supplementary data associated with this article can be found, in the online version, at https://doi.org/10.1016/j.ijheatmasstransfer.2018.01.098.

References

[1] C.D. Holder, The relationship between leaf hydrophobicity, water droplet retention, and leaf angle of common species in a semi-arid region of the western United States, Agr. Forest Meteorol. 152 (2012) 11–16.
[2] P.J. Holloway, M.C. Butler Ellis, D.A. Webb, N.M. Western, C.R. Tuck, A.L. Hayes, P.C.H. Miller, Effects of some agricultural tank-mix adjuvants on the deposition efficiency of aqueous sprays on foliage, Crop Prot. 19 (2000) 27–37.
[3] G.J. Dorr, W.A. Forster, L.C. Mayo, S.W. Mccue, D.M. Kempthorne, J. Hanan, I.W. Turner, J.A. Belward, J. Young, J.A. Zabkiewicz, Spray retention on whole plants: modelling, simulations and experiments, Crop Prot. 88 (2016) 118–130.
[4] M. Massinon, N.D. Cock, W.A. Forster, J.J. Nairn, S.W. Mccue, J.A. Zabkiewicz, F. Lebeau, Spray droplet impaction outcomes for different plant species and spray formulations, Crop Prot. 99 (2017) 65–75.
[5] E.C. Kumbur, K.V. Sharp, M.M. Mench, Liquid droplet behavior and instability in a polymer electrolyte fuel cell flow channel, J. Power Sources 161 (2006) 333–345.
[6] A. Theodorakakos, T. Ous, M. Gavaises, J.M. Nouri, N. Nikolopoulos, H. Yanagihara, Dynamics of water droplets detached from porous surfaces of relevance to PEM fuel cells, J. Colloid Interf. Sci. 300 (2006) 673–687.
[7] B.S. Sikarwar, N.K. Battoo, S. Khandekar, K. Muralidhar, Dropwise condensation underneath chemically textured surfaces: simulation and experiments, J. Heat Trans. – T. ASME 133 (2011) 021501.
[8] X.L. Liu, P. Cheng, Dropwise condensation theory revisited: Part II Droplet nucleation density and condensation heat flux, Int. J. Heat Mass Tran. 83 (2015) 842–849.
[9] K.S. Chen, Modeling water-droplet detachment from GDL/Channel interface in PEM Fuel Cells, in: ASME 2008 – 6th International Conference on Fuel Cell Science, Engineering and Technology, 2008, pp. 797–803.

[10] S.C. Cho, W. Yun, K.S. Chen, Droplet dynamics in a polymer electrolyte fuel cell gas flow channel: forces, deformation, and detachment. I: Theoretical and numerical analyses, J. Power Sources 206 (2012) 119–128.
[11] J. Fan, M.C.T. Wilson, N. Kapur, Displacement of liquid droplets on a surface by a shearing air flow, J. Colloid Interf. Sci. 356 (2011) 286–292.
[12] P. Dimitrakopoulos, J.J.L. Higdon, On the gravitational displacement of three-dimensional fluid droplets from inclined solid surfaces, J. Fluid Mech. 395 (1999) 181–209.
[13] D. Richard, D. Quere, Viscous drops rolling on a tilted non-wettable solid, Europhys. Lett. 48 (3) (1999) 286–291.
[14] L. Mahadevan, Y. Pomeau, Rolling droplets, Phys. Fluids 11 (9) (1999) 2449–2453.
[15] B.S. Yilbas, A. Al-Sharafi, H. Ali, N. Al-Aqeeli, Dynamics of a water droplet on a hydrophobic inclined surface: influence of droplet size and surface inclination angle on droplet rolling, RSC Adv. 7 (2017) 48806–48818.
[16] S.P. Thampi, R. Adhikari, R. Govindarajan, Do liquid drops roll or slide on inclined surfaces?, Langmuir 29 (2013) 3339–3346
[17] O. Wind-Willassen, M.P. Sorensen, A finite-element method model for droplets moving down a hydrophobic surface, Eur. Phys. J. E. 37 (2014) 65.
[18] B.J. Qi, J.J. Wei, L. Zhang, H. Xu, A fractal dropwise condensation heat transfer model including the effects of contact angle and drop size distribution, Int. J. Heat Mass Tran. 83 (2015) 259–272.
[19] M.H. Ran, C.X. Yang, Y. Fang, K.K. Zhao, Y.Q. Ruan, J. Wu, H. Yang, Y.F. Liu, Model for rolling angle, J. Phys. Chem. C 116 (2012) 8449–8455.
[20] S. Basu, K. Nandakumar, J.H. Masliyah, A model for detachment of a partially wetting drop from a solid surface by shear flow, J. Colloid Interf. Sci. 190 (1997) 253–257.
[21] C.H. Schillberg, S.G. Kandlikar, A review of models for water droplet detachment from the gas diffusion layer-gas flow channel interface in PEMFCs, in: 2007 ASME – Proceedings of the Fifth International Conference on Nanochannels, Microchannels and Minichannels, 2007, 30029.
[22] P. Polverino, A. Esposito, C. Pianese, Experimental validation of a lumped model of single droplet deformation, oscillation and detachment on the GDL surface of a PEM fuel cell, Int. J. Hydrogen Energy 38 (2013) 8934–8953.
[23] S.C. Fu, W.T. Leung, C.Y.H. Chao, Detachment of droplets in a fully developed turbulent channel flow, Aerosol Sci. Tech. 48 (2014) 916–923.
[24] F.Y. Zhang, X.G. Yang, C.Y. Wang, Liquid water removal from a polymer electrolyte fuel cell, J. Electrochem. Soc. 153 (2) (2006) A225–A232.
[25] Y. Suh, C. Lee, A numerical method for the calculation of drag and lift of a deformable droplet in shear flow, J. Comput. Phys. 241 (2013) 35–57.
[26] K. Ceylan, A. Altunbas, G. Kelbaliyev, A new model for estimation of drag force in the flow of Newtonian fluids around rigid or deformable particles, Powder Technol. 119 (2001) 250–256.
[27] J. Almedeij, Drag coefficient of flow around a sphere: Matching asymptotically the wide trend, Powder Technol. 184 (2008) 218–223.
[28] V.E.B. Dussan, R.T.P. Chow, On the ability of drops or bubbles to stick to non-horizontal surfaces of solids, J. Fluid Mech. 137 (1983) 1–29.
[29] B.S. Sikarwar, S. Khandekar, K. Muralidhar, Mathematical modelling of dropwise condensation on textured surfaces, Sadhana 38 (6) (2013) 1135–1171.
[30] F. Xing, J.L. Xu, J. Xie, H. Liu, Z.X. Wang, X.L. Ma, Froude number dominates condensation heat transfer of R245fa in tubes: effect of inclination angles, Int. J. Multiphase Flow 71 (2015) 98–115.
[31] H. Ding, E.Q. Li, F.H. Zhang, Y. Sui, P.D.M. Spelt, S.T. Thoroddsen, Propagation of capillary waves and ejection of small droplets in rapid droplet spreading, J. Fluid Mech. 697 (2012) 92–114.
[32] C.L. Yaws, Chemical Properties Handbook, McGraw-Hill, USA, 1999.
[33] A. Hölzer, M. Sommerfeld, Lattice Boltzmann simulations to determine drag, lift and torque acting on non-spherical particles, Comput. Fluids 38 (2009) 572–589.
[34] A.I. Elsherbini, A.M. Jacobi, Liquid drops on vertical and inclined surfaces II. A method for approximating drop shapes, J. Colloid Interf. Sci. 273 (2004) 566–575.